Journal of Natural Gas Science and Engineering 76 (2020) 103196

Contents lists available at ScienceDirect

Journal of Natural Gas Science and Engineering

journal homepage: http://www.elsevier.com/locate/jngse

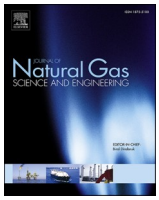

Geological performance evaluation of CO_2 sequestration in depleted oil reservoirs: A simulation study on the effect of water saturation and vertical to horizontal permeability ratio

Rashid Mohamed Mkemai *, Bin Gong

Department of Petroleum Engineering, Faculty of Earth Resources, China University of Geosciences, Wuhan, 430074, Hubei, PR China

ARTICLE INFO

Keywords:
Anthropogenic CO_2
Geological CO_2 storage
Reservoir water saturation
3D numerical simulation

ABSTRACT

Human consumption of fossil fuel as a primary source of energy has led to the net increase of anthropogenic carbon dioxide (CO_2) emission into the atmosphere. The magnitude of its contribution to global warming and climate change is unprecedented. Carbon capture and storage (CCS) in geological formations technology has merged as the key approach towards potential CO_2 sequestration, and depleting oil and gas reservoirs appear to be promising candidates. Various researchers studied the concepts and processes about reservoirs' performance upon CO_2 injection and storage with little attention on variations of reservoir water saturation and permeability ratio (vertical versus horizontal permeability). In this study, with the use of 3-dimensional (3D) numerical simulations the safe and long term evaluation of reservoir performance on CO_2 storage in terms of storage capacity, trapping mechanism, injection rate, and operational pressures were performed at Liaohe basin, China. Results revealed that CO_2 stored in a supercritical form was dominant of all and that at the end of 100 years more than 70% of injected CO_2 existed as free gas in supercritical form, the tendency which decreased to less than 65% after 1000 years of its storage. Conversely, the storage of CO_2 in trapped and dissolved forms was increased by 6% and 3% respectively. The results from this work provide valuable insights on CO_2 phase relative storage potentiality for enhanced and safe CO_2 storage in a depleted oil reservoir. It also provides an improved long term CO_2 storage sequestration strategy which incorporated hysteresis metrics. The study recommends an optimum CO_2 storage scheme with controlled pressure buildup in a depleted oil reservoir.

1. Introduction

The world's energy demand increase is directly proportional to the global population growth and it is entirely tied up with global social and economic development (World Bank, 2017). Fossil fuels (coal, oil, and gas) extraction and burning practices performed by human beings to date have been by far the most common way to satisfy the energy needs in modern economies since the start of the industrial era (IPCC, 2013; World Bank, 2017). However, these activities have generated a tremendous amount of CO_2 into the Earth's atmosphere (Rotty, 1983; IPCC, 2013). According to the World Bank (2017) estimates, 81% of the world's energy production in 2014 was supplied by fossil fuel. The burning of fossil fuels indubitably leads to the emission of greenhouse gases. The major component of greenhouse gases emitted into the atmosphere is CO_2, which accounts for approximately 64% of the greenhouse gases (Bachu, 2000). Its concentration in the atmosphere is continuously increasing to the extent that it approaches one half of its pre-industrial era (IPCC, 2013). Records reveal that CO_2 concentration by volume was 404 parts per million volume (ppmv) in 2016, while the pre-industrial concentration was 280 ppmv, about 50% increment (IPCC, 2013; EPA, 2017). If immediate and appropriate mitigation measures are not taken, it may lead to serious global climatic changes and disruptions. Carbon capture and storage (CCS) appears as the most recent and promising strategy that can be adopted to overcome the existing challenge. The technique involves the application of technology to capture carbon dioxide, transporting it to an appropriate place, and finally, store it beneath the Earth's surface for long-term isolation from the atmosphere (IPCC, 2005). The main geological sites for CCS include deep saline formations, mature and depleted oil and gas fields, unmined coal bed formations, and mined salt domes (IPCC, 2005; Raza et al., 2016b). The deep saline aquifers are naturally widely spread and possess a huge potential of storing anthropogenic CO_2 (IPCC, 2005). But the fact

* Corresponding author.
E-mail addresses: mkemai2000@yahoo.com (R.M. Mkemai), gongbin@tracyenergy.cn (B. Gong).

https://doi.org/10.1016/j.jngse.2020.103196
Received 10 November 2019; Received in revised form 7 January 2020; Accepted 3 February 2020
Available online 6 February 2020
1875-5100/

that little exploration work has been done worldwide to ascertain its storage capacity and its economic viability has been a challenge (Leung et al., 2014; Zhang, 2015). Depleted oil and gas reservoirs have shown substantial results in terms of storage integrity, safety, economy and environmental friendliness as compared to other CO_2 storage options, such as enhanced coal-bed methane, ocean and deep aquifers (Lai et al., 2015; Zhang and Huisingh, 2017). Its application has been reported attractive due to several reasons including detailed explored geology with sufficient information related to its properties, fluid contents, and characteristics that were previously captured during its operation era, another reason is possession of sufficient overburden which discourages shallower resources contamination and increased safety insurance. Moreover, they experienced different varying subsurface conditions such as elevated pressure, temperature, and stresses for sound field operation time. Further, they have favorable CO_2 injection conditions such as supercritical temperature and pressure, and have available useful surface and sub-surface facilities and infrastructure which can be adopted and customized to fit into CO_2 storage projects and incremental oil recovery (CO_2-EOR) at reasonable additional costs. (Bachu and Adams, 2003; Lai et al., 2015; Raza et al., 2016a; Aminu et al., 2017; Jia et al., 2018). Table 1, show examples of the US sequestration storage records presenting attractiveness and suitability of oil and gas reservoirs as far as storage integrity and environmental risk potentiality is concerned (Shukla et al., 2010).

Various researchers studied the potential of reservoir performance on CO_2 injection and storage through numerical modeling and simulation. Maneeintr et al. (2017) employed simulation models to study CO_2 injection and its related fluid dynamics in a depleted oil field in the Northern part of Thailand. Results showed that the sequestration process was successful and that injection parameters were within the designed safe project storage limits. Therefore, the flow rate was within the designed range to cause formation damage and pressure build-up didn't reach its maximum allowable pressure of 32.29 MPa. Raza et al. (2016b) presented a method of estimation of CO_2 residual saturation during the trapping mechanism process. The method described restriction of CO_2 movement in the reservoir to ensure optimized long term safety of the injected fluid. Moreover, it was observed that increasing salinity and injection pressure led to increased amount of free and residual CO_2. In optimizing CO_2 sequestration and enhanced oil recovery Dai et al. (2013) developed an integrated framework for a depleted oil reservoir in Texas. Using field parameter distributions, they simulated multi-phase, multi-component and reactive fluid flow with the use of multiphase reservoir simulator SENSOR (CEI, 2011), geologic models and statistical data. Results indicated that reservoir petrophysical parameters (mainly porosity and permeability), reservoir thickness and depth were the principal controller of CO_2 injection, sequestration and recovery rate for oil/gas. Moreover, it was revealed that the distance between injection and production wells and the sequence of alternating water and CO_2 injected played a vital role for a five-spot CO_2-EOR project design. Welkenhuysen et al. (2017), developed a techno-economic simulator to forecast and assess feasibility and practicability of CO_2-EOR offshore project in the North Sea. They used limited foresight together with Real Options Analysis to guide on decision making which involves investment on projects regardless of the project's degree of uncertainties and risk. And it was observed that different oil field can be analyzed as a single group project to reduce investment difficulties. Jiang et al. (2019) developed an integrated model to assess CO_2 EOR technical and economic performance based on historical field data. Six scenarios with varying design parameters were simulated under the net present value variable. Based on sensitivity analysis it was revealed that the net pay, porosity, oil saturation, CO_2 injection, depth and oil formation factor were the key parameters in the economic performance of the CO_2 EOR project. Dai et al. (2016) performed CO_2 accounting and risk analysis for a commercial CO_2-EOR project at the Farnsworth Unit, Texas. The study explored CO_2 storage potential and its economic and environmental risks. Multiple scale statistical framework was developed and simulations were run to quantify uncertainty boundaries of the risk involved. Their results showed profit viability from the economic model. In a continual effort to study performance and prediction of CO_2 storage, Jia et al. (2018) generated 50 realizations by using a sequential Gaussian simulation approach to describe the variation of porosity and permeability in the reservoir based on site seismic survey and well logs data. In their work, they studied the impact of 3-phase relative permeability as well as hysteresis models on forecasting storage in CO_2-EOR projects. Among other important simulation results of the study revealed that CO_2 storage capacity was affected by the choice of the model and that there was a small impact on CO_2 trapping during CO_2-EOR injection period as compared to post injection period where it was observed to rise. Ampomah et al. (2016) performed CO_2 storage numerical simulation for a CO_2 enhanced oil recovery site in the Morrow sandstone reservoir in the Farnsworth Unit, Texas. In their study, they evaluated CO_2 Storage Mechanisms and tested different hypothetical injection schemes. They observed that residue oil accommodated a significant amount of CO_2 injected. Moreover, supercritical-phase CO_2 amounts in the reservoir depended on the CO_2 injection scheme, furthermore, it was revealed that hysteresis had a significant impact on residual trapping. Parameters such as pressure, reservoir fluid volume, water-alternating-gas (WAG) schemes, and caprock integrity showed a substantial contribution in CO_2 storage capacity. It was finally concluded that caprock integrity had enough storage and withstanding capacity. Raza et al. (2018) studied the effect of residual gas on the injection process through the use of simulation models, results showed proportionality between residual gas quantity and reservoir fluids in the formation. According to IPCC (2005), the storage of CO_2 in geological formations is mainly achieved through injection of the fluid via ground created wells in both onshore and offshore basins. Injection is done when CO_2 is in its supercritical condition. The trapping mechanism for CO_2 storage process are mainly: (i) structural and stratigraphic trapping, which occurs when CO_2 plume migration is trapped by the seal or impermeable rock, (ii) residual trapping, which obeys the principle of fluid displacement mechanism, where CO_2 displaces fluid in the pores of the reservoir formation and renders it immobile within pore spaces (Aminu et al., 2017), (iii) solubility trapping, where CO_2 dissolves in brine water in the reservoir formation causing density increment and lowering of pH of the contacted brine water (Xu et al., 2004), (iv) mineral trapping, which involves the process of turning CO_2 immobile by geochemical reactions that it undergoes with carbonate minerals, leading to chemical precipitations of immobile secondary carbonate phases. This process is slow and takes a long time, which may span considerable geological time (Hellevang et al., 2017).

In this study, a 3-dimensional (3D) homogeneous reservoir model was built and reservoir layer storage performance was analyzed based on field data. Reservoir CO_2 storage performance in terms of storage capability, trapping mechanism incorporating hysteresis influences, injection rate, and operational pressures was performed with the application of 3D numerical simulations. Generalized Equation of State Model Reservoir Simulator (GEM) from the CMG - Computer Modeling

Table 1
Storage capacities and potential environmental risks associated with various forms of CO_2 geological storage.

Storage Strategy	Capacity (Gt-CO_2)	Storage integrity	Environmental potential risk
Depleted oil and gas fields	25–30	High	Low
Active oil wells (EOR)	Low	High	Low
Enhanced coal-bed methane	5–10	Medium	Medium
Deep aquifers	1–150	Medium	Medium
Ocean (global)	1000–10,000	Medium	High
Carbonate storage (no transport)	Very high	Highest	High

Group (CMG-GEM, 2012) has been employed to perform simulations for 1000 years. The simulator proved a strong capability to model CO_2 sequestration mechanisms in both saline aquifer and CO_2-enhanced oil recovery (CO_2-EOR) processes. It is a multiphase, multicomponent, compositional simulator solving a variety of fluid dynamic processes of miscible and immiscible injection, including phase physical and chemical equilibrium reactions, centered on a fully coupled and adaptive implicit approach (Nghiem et al., 2004).

The main objective of this article is to present multiphase, multicomponent reservoir simulations describing typical CO_2 storage trapping mechanisms based on CO_2 phase relative storage potentiality for enhanced and safe CO_2 storage in a depleted oil reservoir at Liaohe basin, China. It shows CO_2 phase storage, spatial distribution and its migration in relation to reservoir water saturation and permeability changes in vertical and horizontal directions. Moreover, it provides an enhanced safe and long term CO_2 storage sequestration technique that incorporated hysteresis metrics. Further, it gives invaluable insights on performing CO_2 injection processes at pressure-controlled mode to limit reservoir pressure build-up which may trigger fracture and faults activities. The study provides a base and serves as a reference for storage projects in depleting oil reservoirs at Liaohe basin and projects of similar geological settings nature in the world.

2. Methods

2.1. Geological description of the study area

Liaohe basin in China is the largest heavy and extra heavy oil field and the third-largest oil-producing region in the country. It is located in the North-Eastern part of the Bohai bay rift basin series, with an exploration area of 12,400 km^2 (Zhu et al., 2010). Shen 84 Block is within the Liaohe basin in the Jinganbao oil-rich structural region of Damingtun depression in Xinmin city (Liaoning Province) (Fig. 1). Shen 84 is a faulted structure, anticlined in nature and occupying an area of approximately 2.24 km^2. It is of the Paleogene period (Eocene) of Shahejie formation. It has a complex depositional system characterized by fluvial and deltaic origin with some small sand body (Peng et al., 2014).

Table 2, shows a generalized stratigraphy of the Damingtun depression. The average formation depth is at 2015 m and the minimum reservoir depth is 1000 m from the ground surface. This depth is very significant as it allows CO_2 injection in its supercritical state. Liaohe Oilfield formation has been spotted for CO_2 injection since 1998, therefore, since then several pilot-scale projects related to enhanced oil recovery and CO_2 injection have been tested and conducted with comprising results (Jin et al., 2012). The average porosity of the formation is 20.9%, and its permeability is 3×10^{-3} μm^2 (3 mD). The average formation pressure and temperature are 19.5 MPa and 67.5 °C respectively.

Table 2
Generalized stratigraphy of Damingtun depression (modified after Xiaoguang and Zuan (1991)).

Age/ System	Formation	Member	Formation lithology	Thickness (m)
Paleogene	Dongying		Sandy conglomerate	500±
	Shahejie	Sha-1	Mudstone, gas, sandstone	500–1000
		Sha-3	Mudstone, oil, gas, sandstone, sand conglomerate	1500 - 3500+
		Sha-4	Mudstone, oil, oil shale, basalt	300 - 1500+
Cretaceous			Sandstone	0–40
Proterozoic	Gaoyuzhuang	Gao-1	Quartzite, oil-bearing fractures	0–1000+
		Gao-2	Dolomite, oil-bearing fractures, clay slate, quartzite	
		Gao-3	Dolomite, oil-bearing fractures	
	Dahongyu		Dolomite, oil-bearing fractures	
Archean			Oil-bearing fractures, metamorphic rocks, lamprophyre, diabase	

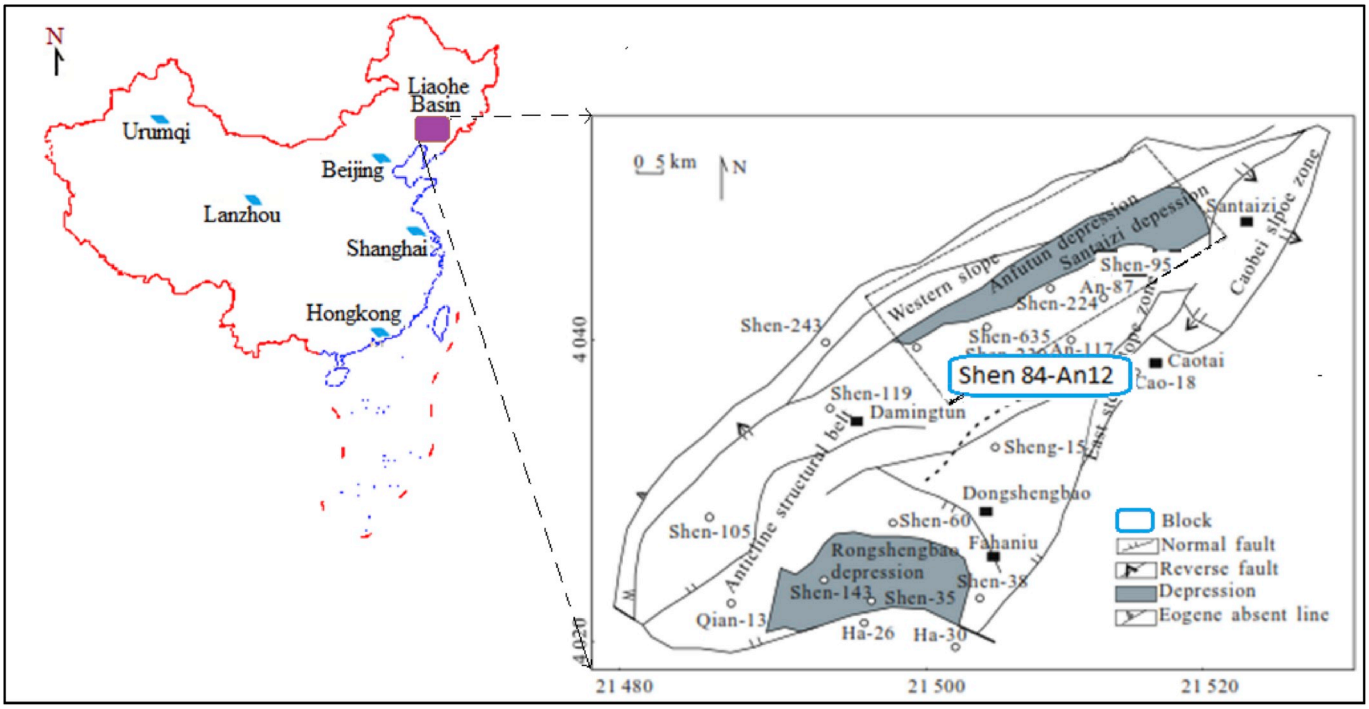

Fig. 1. The geological description of the study area Block Shen95, modified from Zhu et al. (2010).

2.2. Numerical simulation method

Generalized Equation of State Model Reservoir Simulator (GEM) from the CMG - Computer Modeling Group (CMG-GEM, 2012) has been used to perform simulations in this study. The GEM simulator has a great ability to model various important mechanisms involved in CO_2 sequestration as well as enhanced hydrocarbon recovery processes. It is a 3-Dimension, multiphase, multicomponent, numerical compositional simulator solving variety of mechanisms of miscible and immiscible gas injection process, including phase physical and chemical equilibrium reactions such as mineral dissolution/precipitation, swelling of oil, viscosity reduction along with multiphase multicomponent mass transfer, which is centered on a fully coupled and adaptive implicit approach (Nghiem et al., 2004).

2.3. Mathematical fluid flow models

The dynamics of CO_2 flow and transport with its interaction with porous media are governed by mass and momentum conservation laws. The equations governing the dynamics of multi-phase flow under the isothermal condition is controlled by a combination of some very crucial partial differential equations (Liu et al., 2014).

$$\frac{\partial M^{\kappa}}{\partial t} = -\nabla . F^{\kappa} + q^{\kappa} \tag{1}$$

where M is the mass buildup in the system (kg/m^3), F is the mass flux (kg/m^2 s), q is the source or sink (kg/m^3 s), t is time in seconds, ∇ is the divergence, κ one of the mass components such as CO_2, air and water.

If Eq. (1) involves water component in the fluid system, the following governing equation is used

$$\frac{\partial}{\partial t}\left[\phi\left(X_l^w S_l \rho_l + X_g^w S_g \rho_g\right)\right] = -\nabla .\left\{X_l^w \rho_l\left(-k\frac{k_{rl}}{\mu_1}(\nabla P_l - \rho_l g)\right) + X_g^w \rho_g\left(-k\frac{k_{rg}}{\mu_g}(\nabla P_g - \rho_g g)\right)\right\} + \left(q_l^w + q_g^w\right) \tag{2}$$

where ϕ is the porosity, X_l with superscript w is the mass fraction of component w in phase l, S is the saturation, g is the gravitational acceleration [LT^{-2}], w represents water, k is permeability [L^2], ρ is a density [ML^{-3}], k_{rg} refers to a relative permeability, P stands for pressure [ML^{-1}T^{-2}], l, g and s stand for liquid, gas and solid phases respectively and μ is the viscosity [ML^{-1}T^{-1}]. The governing equations for the CO_2 component in the multiple phase fluid systems can be rewritten as:

$$\frac{\partial}{\partial t}\left[\phi\left(X_l^c S_l \rho_l + X_g^c S_g \rho_g\right)\right] = -\nabla .\left\{X_l^c \rho_l\left(-k\frac{k_{rl}}{\mu_1}(\nabla P_l - \rho_l g)\right) + X_g^c \rho_g\left(-k\frac{k_{rg}}{\mu_g}(\nabla P_g - \rho_g g)\right)\right\} + \left(q_l^c + q_g^c + q_s^c\right) \tag{3}$$

where c stands for CO_2

Eq. (3) is the key governing equation describing the composition of CO_2 in three-phase fluid systems.

2.4. Model descriptions and setup

The reservoir parameter and properties of the site as shown in Table 3 were used to construct the numerical model. The developed 3D homogeneous compositional model was numerically simulated based on field dimensions of 2.8 km by 0.8 km at a total formation thickness of 106 m. The average porosity was 20.9% and horizontal permeability (K_h) was 3 mD (Orodu et al., 2009; Peng et al., 2014). The ratio of vertical to horizontal permeability (K_v/K_h) was 0.1 for the base case (Kasap, 2001). The main reason for setting the permeability ratio was based on the model restriction on vertical fluid flow. K_v/K_h ratio is an important fluid flow factor when creating consistent models for anticipating field performances. When it is greater than 1, more flow takes place in a vertical direction as compared to the horizontal direction and when it is less than 0.1 more restrictions are set to the fluid flow in a vertical direction. Moreover, as discussed by Kasap (2001), an empirically derived K_v/K_h ratio of 0.1 is commonly recommended in the industry to account for the fluid flow movement.

Table 3
Reservoir rock and fluid petrophysical properties and its hydrogeological parameters (Orodu et al., 2009; Peng et al., 2014; Yang et al., 2018a).

Rock properties		Fluid properties	
Property/Parameter (units)	Value	Property/Parameter (units)	Value
Reservoir dimensions	2800 × 800 x 106	Water saturation, Sw (%)	50
Grid size	30 × 25 x 6	Initial oil saturation	50
Average Perm, K (μm^2)	0.53	Water density (kg/m^3)	1030
Porosity, (%)	20.9	Water viscosity (cp)	0.5
Perm. V/Perm. H, Kv/Kh	0.1	Formation water salinity, (mg/L)	10,000
Reservoir temperature, (°C)	67.5	Oil specific gravity (kg/m^3)	870
Initial reservoir pressure (MPa)	19.5		
Formation depth (m)	1000		
Rock compressibility (/kPa)	3.03 × 10^{-8}		

Thus, different values for K_v/K_h ratios were tested to study its effect on the storage capacity and performance of the reservoir. Reservoir depth with reference to the surface was at 1000 m and the initial reservoir pressure was 19.5 MPa. Initial water saturation of 50% was recorded, and the formation water salinity was 10,000 ppm. The model was assumed to be isothermal at 67.5 °C and there was no dissolved gas at the beginning, except during the injection process. Moreover, the process of the geochemical reaction was not taken into account during modeling. The model grids were designed at 30 cells × 25 cells x 6 cells for the x-y-z directions, making the total grid block equals to 4500 cells. The model is a sandstone reservoir with low permeability and zero dip. Additionally, it was assumed that CO_2 injection was conducted at supercritical conditions.

2.5. Rock-fluid properties

Water-gas relative permeability parameters are vital data during model simulation processes as they provide guidance on the fluid dynamics in the reservoir. Furthermore, they have a significant influence on CO_2 injectivity as the formation region around the wellbore is normally high water saturated (Liu et al., 2010). In this study, Van Genuchten (1980) and Corey (1954) functions applicable in sandstone and mudstone were adopted to estimate relative permeability of aqueous phase and gas in the reservoir. Additionally, Van Genuchten's functional form was applied to estimate capillary pressure curves (Akaku, 2008; Liu et al., 2010). The curves representing relative permeability for the rock-brine-CO_2 used in this study are shown in Fig. 2(a) and (b).

In the model, well injector location was at block (x, y) = (15, 13), of which the flow process was centered. The vertical injector well was perforated and located at block model position (x, y, z) equals to (15, 13, 2–6), with the depth from 1010 m to 1060 m. Pure supercritical CO_2 was injected for 10 years followed by 100 years of a shut-in. Further, 1000 years post shut-in was simulated to study the long term effect and spatial distribution of CO_2 storage under different forms within the reservoir. The reservoir model constraints were set at maximum bottom hole pressure (BHP) of 35 MPa and a maximum injection rate of 2500m^3/day at standard conditions of pressure and temperature.

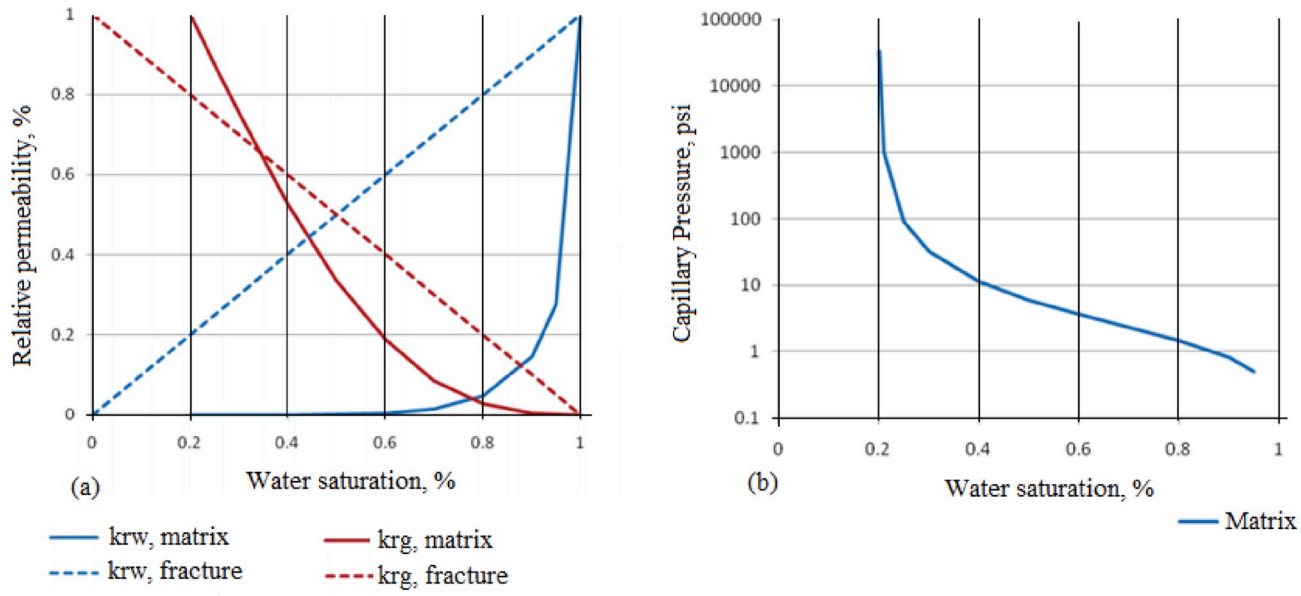

Fig. 2. (a) Relative permeability curve (b) A curve for reservoir capillary pressure.

2.6. Reservoir model construction and fluid phase behavior descriptions

Fluid modeling was performed by using the Peng-Robinson equation of state (EOS) for typical fluid from Liaohe Oilfield. Table 4 presents the fluid model parameters used in the study. CMG-WinProp was employed to describe the properties and phase behavior of reservoir fluids (CMG-WinProp, 2012).

2.6.1. CO_2 solubility in the brine

Peng-Robinson Equation of State (Peng and Robinson, 1976b) was tuned to fit the site available experimental data as presented in the study performed by Yang et al. (2018b). The reservoir fluid component properties such as density, pressure, and temperature as well as CO_2 solubility, brine density and viscosity were estimated by using the same Peng-Robinson equation of state. The dissolution of CO_2 was estimated through Henry's law (Li and Nghiem June, 1986) for brine at a salinity of 10,000 ppm. The dissolution rate in the brine was assumed to be in thermodynamic state of equilibrium and its equation is the equality of fugacities of the component in CO_2 and brine (Nghiem et al., 2004), that is,

$$g_i = f_{ig} - f_{iw},\ I = 1 \ldots n_g \tag{4}$$

Equation (4) is mainly applicable when injected CO_2 is not 100% pure, meaning that it is mixed up by some components n_g. Again Peng-Robinson equation was employed to calculate fugacity f_{ig}. Henry's law (Peng and Robinson, 1976a) was used to estimate the fugacity of gaseous components dissolved in brine, that is,

$$f_{iw} = y_{iw}.\ H_i, \tag{5}$$

where H_i in eq. (5) is Henry's constant which it's set up was conducted by assuming that only CO_2 dissolved in the system. It was also assumed that the formation is an open system meaning that apart from vertical movement of injected CO_2 it can also migrate horizontally in the layers after shut-in. The phase viscosity of the brine was estimated by using Rowe and Chou (1970) correlation and Kestin et al. (1981) correlation.

Reservoir fluid model results after fluid model lumping, splitting and regression are shown in Table 5. As it was sourced from the study conducted by Yang et al. (2018b) at Liaohe Oilfield.

Table 4
Reservoir compositional fluid system and parameters (Yang et al., 2018b).

Component name	Mole (%)	Pc (atm)	Tc (K)	Acentric factor	Molecular Weight
CO_2	0.020	72.800	304.200	0.2250	44.0
N_2 - CH_4	20.539	45.045	188.488	0.0090	16.4
C_2 - C_5	3.600	39.357	401.770	0.1757	52.6
C_6 - C_{12}	22.654	19.917	613.414	0.4235	130.0
C_{13} - C_{35}	42.140	13.709	797.799	0.8515	299.7
C_{36+}	11.047	5.227	1262.265	1.6124	1415.0

3. Simulation results and discussion

After 1000 years post-injection of CO_2, the higher concentration level of CO_2 was observed at the upper part of the reservoir below its cap-rock as can be seen in Fig. 4. The accumulation was mainly due to the buoyancy effect of CO_2 plume which led to its spread and accumulation beneath the seal rock of the reservoir (Agada et al., 2017). As more CO_2 was injected through the wellbore, more pressure was created in the reservoir especially beneath the seal rock. With the impermeable seal rock layer, the lateral spread of the CO_2 plume was a necessary option for the plume. The intensity of the gas accumulated below the seal rock varies depending on factors such as time of storage and reservoir layers' permeability. It can be seen that gas saturation at the top of the reservoir in the early 100 years was lower at approximately 0.6–0.7 as compared with the saturation at 1000 years, where the saturation range was 0.7–0.8 (see Fig. 3).

Fig. 5(a) shows the reservoir dimensions and the location of the injector well, and Fig. 5(b) is the global CO_2 mole distribution display indicating that within 100 years most of the injected gas was trapped as free gas in its supercritical state.

It was observed in both cases (100 and 1000 years post shut-in) that there was an immediate decrease in bottom hole pressure after the shut-in of the wellbore (Fig. 6). This was possibly associated with two factors (i) dissolution of CO_2 in the brine and (ii) its imbibition as it got trapped in the reservoir pores during its insitu migration processes horizontally and vertically (Basbug and Gumrah, 2007). Moreover, the gas rate at surface conditions rose slowly to its peak and then dropped to zero at the time of shut-in.

3.1. Difference in CO_2 phase storage capacity and trapping mechanism

The CO_2 stored in the reservoir was in three different forms (i) free/

Table 5
Compositional reservoir parameters based on the reservoir system.

Component	Mole (%)	Pc (atm)	Tc (K)	Acentric factor	Molecular Weight	Omega A	Omega B	SG
CO_2	0.020	72.800	304.200	0.2250	44.01	0.4572	0.0778	0.8180
N_2 to CH_4	20.539	39.743	158.406	0.0236	21.87	0.4572	0.0778	0.4937
$CH_2$to NC_5	3.600	39.339	398.404	0.1709	52.28	0.4572	0.0778	0.5308
C_6 to C_{12}	22.654	26.909	594.723	0.3916	120.48	0.4572	0.0778	0.7636
C_{13} to C_{35}	42.140	12.271	827.599	0.9379	329.94	0.4572	0.0778	0.8887
C_{36+}	11.047	5.227	304.200	1.6124	1415.00	0.4572	0.0778	0.2433

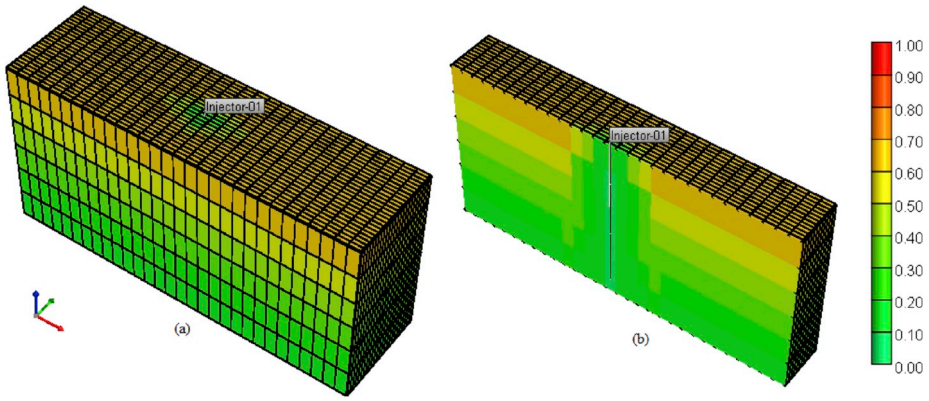

Fig. 3. A 3D spatial CO_2 distribution (a) a full model gas saturation distribution (b) a half model gas saturation distribution stipulating details of gas profiles for 100 years post shut-in.

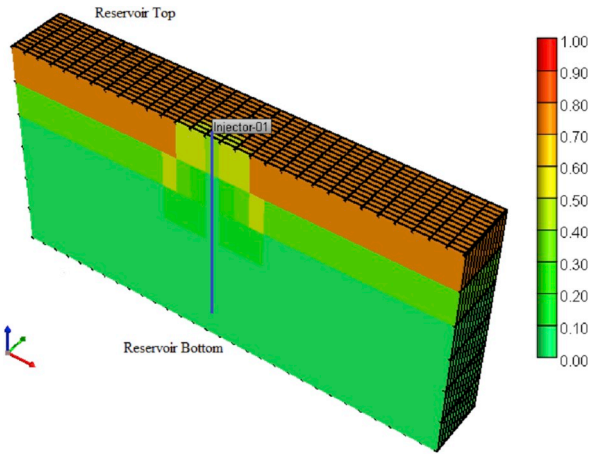

Fig. 4. A half-cut CO_2 spatial distribution gas saturation model showing the inner part of the reservoir 1000 years after the injection process.

supercritical CO_2, (ii) trapped or residual CO_2, and (iii) was a dissolved form of CO_2. Mineral storage is also among the forms in which CO_2 can be stored but it was not covered in this study, this is mainly because the mineral dissolution reaction and precipitation are slow and takes a long time (Nghiem et al., 2009).

It was observed that the variation in water saturation led to varying amounts of CO_2 phase stored in the reservoir. Moreover, CO_2 was observed to be stored at lower water saturation conditions as compared to higher water saturation conditions.

Fig. 7 shows three CO_2 forms stored cumulatively in 100 years period. Simulation results revealed that a total of 6.3×10^8 kg of CO_2 was stored in the reservoir at the water saturation of 0.5, while 5.02×10^8 kg and 4.08×10^8 kg of CO_2 were stored at a water saturation of 0.7 and 0.9 respectively. This indicated a decrease of 20% and 35% of reservoir total storage capacity at 0.7 and 0.9 water saturation respectively as compared to the base case of 0.5 water saturation. The reason for storage capacity decrease may be attributed to the pore space limitation (occupied by water) that would otherwise be taken by CO_2 injected under the constraints of pressure and time. It was observed that for the first 100 years of storage the dominant form of CO_2 stored was in the supercritical phase, followed by trapped/residual, and then dissolved CO_2.

As previously stated that the total amount of stored CO_2 was a combination of three forms: supercritical, trapped/residue and dissolved CO_2. The CO_2 phase which dominated the reservoir in terms of storage ability for 100 years was the supercritical phase followed by trapped/residue and ten dissolved form, its cumulative amount in terms of percent and their corresponding saturation are shown in Fig. 8.

From Fig. 9, it was revealed that the total amount of CO_2 stored in the reservoir in a supercritical form decreased with time as water saturation increased. For instance, the reservoir water saturation of 0.5, 0.7 and 0.9 resulted in total stored supercritical CO_2 of 74%, 70%, and 55% respectively. The decrease of stored supercritical CO_2 with water saturation was mainly caused by dissolution and trapped gas in pores during its migration in the reservoir. On the other hand, it was observed that the amount of CO_2 stored in the trapped and dissolved form increased as the water saturation decreased. For instance, the total amount of CO_2 stored in the trapped form in 100 years post shut-in at saturation of 0.5, 0.7, and 0.9 was recorded as 20.4%, 22.8%, and 36.8% while that of dissolved form was 5.8%, 7.2%, and 7.9% respectively. The additional explanations of the decrease in storage amount of supercritical CO_2 and an increase of trapped and dissolved CO_2 was that injected gas experienced a buoyancy effect which made it finds its way to the roof of the reservoir beneath the seal rock, and during the movement, it gets trapped in the reservoir pores and at the same time dissolved in brine.

Simulation results for 1000 years revealed that there was a decrease of 2% of the total supercritical CO_2 injected as compared to the period of 100 years. However, there was an increase of 26% of residue/trapped CO_2 and 19% dissolved in the brine. These findings are corroborated by some other researchers such as Heinemann et al. (2018) who performed their study on CO_2 sequestration with limited sealing capability in the Pearl River Mouth Basin. Finally, it was observed that as the time elapsed from the date of injection, the amount of supercritical CO_2

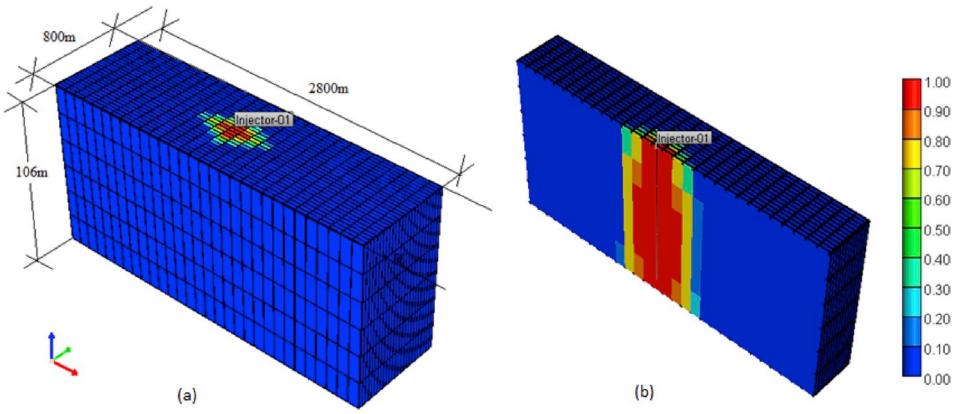

Fig. 5. Reservoir full and a half model showing (a) model dimensions and CO_2 injection well location (b) CO_2 global mole fraction distribution profile, 100 years after shut-in.

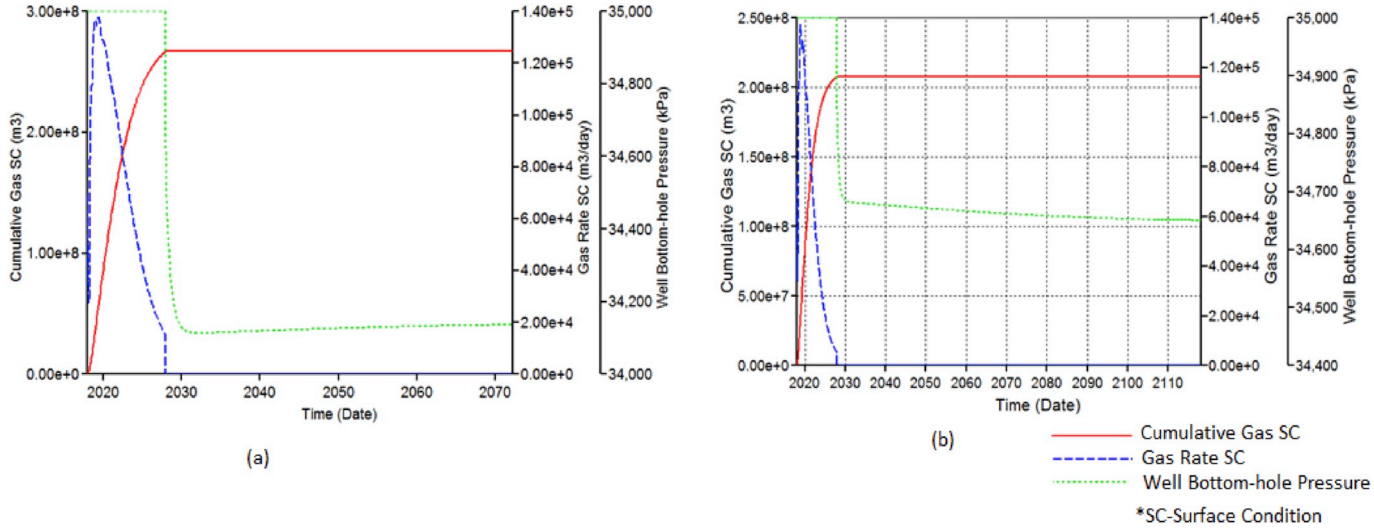

Fig. 6. Injection history profile with peak values of cumulative CO_2 stored (a) 100 years after injection and shut-in, (b) 1000 years after shut-in, zoomed and displayed to 2110.

stored in the reservoir decreased, while the amount of trapped and dissolved CO_2 increased.

Injection rates were observed to vary subject to the level of saturation, and the trending showed a decrease of injection rate towards the shut-in period, Fig. 10. The decrease in injection rate was possibly due to a decrease in pore spaces which were gradually occupied by CO_2 plume during the injection process. Moreover, increased pore pressure which resulted in counter injection pressure was also observed. It was additionally revealed that as the reservoir water saturation increased, the gradient of the CO_2 injection rate became steeper with time. This was mainly due to pore water pressure which exerted an opposed pressure during injection. The ratio of vertical to horizontal permeability (K_v/K_h) was analyzed and its effect was described in the subsequent section.

3.2. Vertical to horizontal permeability ratio (K_v/K_h) effect on CO_2 storage

In this study, the base case K_v/K_h value was 0.1 and the maximum K_v/K_h was at 1 with a step incremental variation of 0.1 as can be stipulated in Table 6. Simulation results revealed that the increase of the K_v/K_h ratio led to an increased amount of trapped CO_2 in dissolved form. Moreover, the amount of CO_2 stored in a residue/trapped form was rising as the permeability ratio increased.

A simulation study conducted for the K_v/K_h ratio of 0.1–1 revealed that the K_v/K_h ratio of 0.1 had a total CO_2 stored amount of 6.28×10^8 kg, while the K_v/K_h ratio of 1 had a total sum of 6.65×10^8 kg CO_2. Fig. 11 displayed the trend of CO_2 stored amount. This implied that there was an increment of 5.8% of CO_2 stored at the K_v/K_h ratio of 1 compared to the K_v/K_h of 0.1 (Table 7).

Simulation results revealed that the amount of trapped/residue and dissolved CO_2 stored in the reservoir was proportional to K_v/K_h ratios while the amount of supercritical CO_2 remained almost unchanged for the entire post shut-in period. A similar observation was reported by Ghanbari et al. (2006). The percentage increase in trapped/residue and dissolved CO_2 was 27.1% and 4.1%, respectively. The increased K_v/K_h ratio implied that a more vertical permeable environment was created, which in turn favored the migration of CO_2 in a vertical direction. The more the vertical migration is favored by increased buoyancy force towards beneath the cap-rock, the more it interacts with the formation brine the then facilitates the dissolution of CO_2.

Fig. 12 was created to have a detailed understanding of behaviors stipulated by three different CO_2 forms stored over the wide range of K_v/K_h ratios. Results showed a constant amount of dissolved and supercritical CO_2 forms stored in a whole period of 100 years of post-shut-in. However, it was observed that cumulative CO_2 stored in the trapped/residue form at K_v/K_h ratio of 20 was 1.27 times that at the K_v/K_h ratio of 0.5. The increase, in this study named region A in Fig. 12, was probably caused by the fact that K_v/K_h ratio at 20 favors gas mobility in the

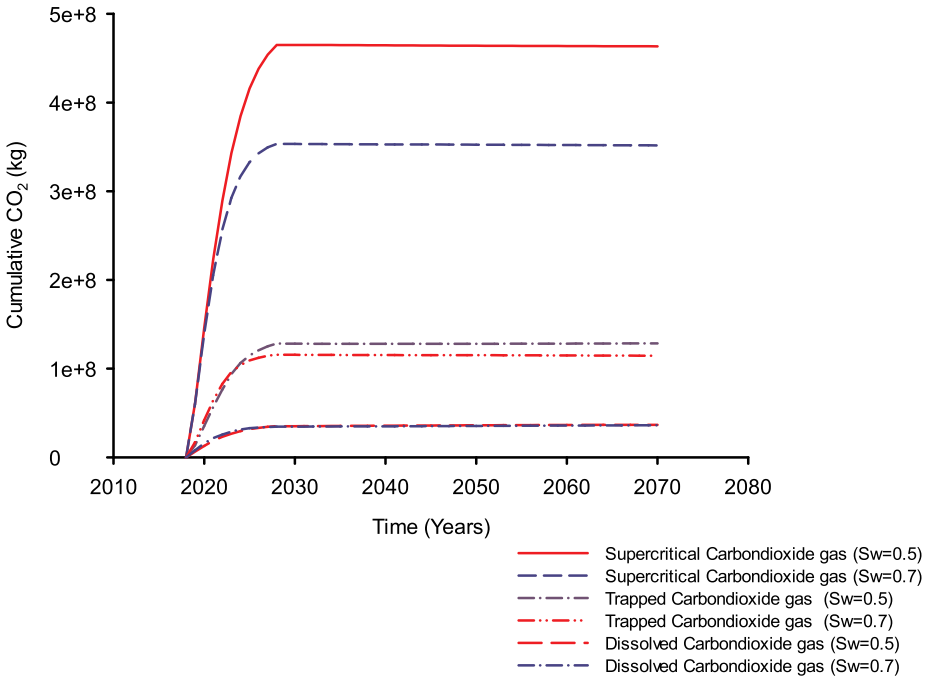

Fig. 7. Cumulative CO_2 storage characteristic curves resulted due to variation in water saturation for 100 years shut-in period.

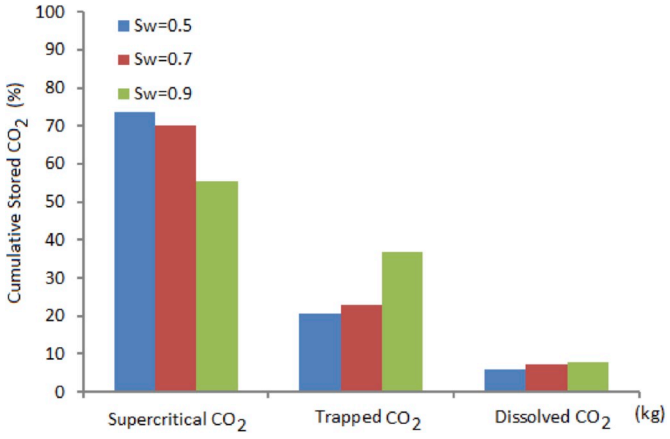

Fig. 8. CO_2 gas stored in supercritical trapped/residue and dissolved form in brine at 0.5, 0.7, and 0.9 water saturation respectively, for 100 years post shut-in.

reservoir and during the gas migration towards the top beneath impermeable rock it displaced brine in pores and hence get trapped. It was also observed that besides the general trend of the increased amount of stored CO_2 with the K_v/K_h ratio, region A had an extraordinary high K_v/K_h ratio for trapped/residue CO_2. For both cases, it was observed that more CO_2 was accumulated below the caprock of the reservoir. The accumulation led to formation pressure build-up, however, the lateral movement of CO_2 reduced the effect and the seal rock crack initiation pressure was controlled not to exceeded the threshold. To this end, the integrity and safety of the reservoir cap-rock was maintained for the entire period of study. Some additional sensitivity parameters were incorporated to explore more about the study, bottom hole pressure (BHP) and salinity were tested. And the following simulation results were observed.

3.3. The effect of salinity

Salinity was tested as shown in Table 8. In the study, 50% salinity was added in one case and reduced in the other. Simulation results revealed that an increase in salinity led to a decreased amount of dissolved CO_2 in the brine. In this case, a 20% reduction from the base case was observed. In contrary, the decrease in salinity resulted in the increased dissolution of injected CO2 as compared to the base case. This observation coincides with studies done by those which was conducted by Ghanbari et al. (2006), Omambia and Li (2010) and Ampomah et al. (2015).

3.4. The effect of bottom hole pressure (BHP)

The BHP was tested by altering about 25% lower and above the base case as shown in Table 8. Simulation results revealed that the decrease of BHP led to a decrease of CO_2 amount stored in the dissolved form, likewise, the increase of BHP resulted in an increase of the dissolved CO_2 in brine as compared to the base case. It was generally observed that as the BHP increases, the amount of dissolved CO_2 in the reservoir also increases. However, monitoring and control of BHP remain to be a very important task as disregarding it may result in reservoir pressure build-up and create initiation of fractures and faults within the reservoir which in turn may trigger gas leakage and endanger the CO_2 storage safety of the site. Nevertheless, increased pressure enhances the interaction between the injected gas molecules and the brine; it also facilitates the lateral movement of supercritical CO_2 in the reservoir.

4. Conclusion

Geological CO_2 sequestration in depleted oil reservoirs is among the very impressive strategy for anthropogenic CO_2 mitigation. It becomes more attractive when the risks and hazards associated with the site geology and environments are minimized or eliminated during and after the process. Risk of CO_2 leakage, pressure buildup, fault activities, and seismicity are crucial to be prior evaluated for the safe and long term storage of CO_2 in a reservoir. This study presents a 3D numerical model that was developed and simulated to analyze reservoir performance and storage capacity for a depleted oil reservoir. Various storage mechanisms were studied and three CO_2 phase storage form analysis with respect to formation water saturation at Jinganbao site was conducted. The following were the findings of the study.

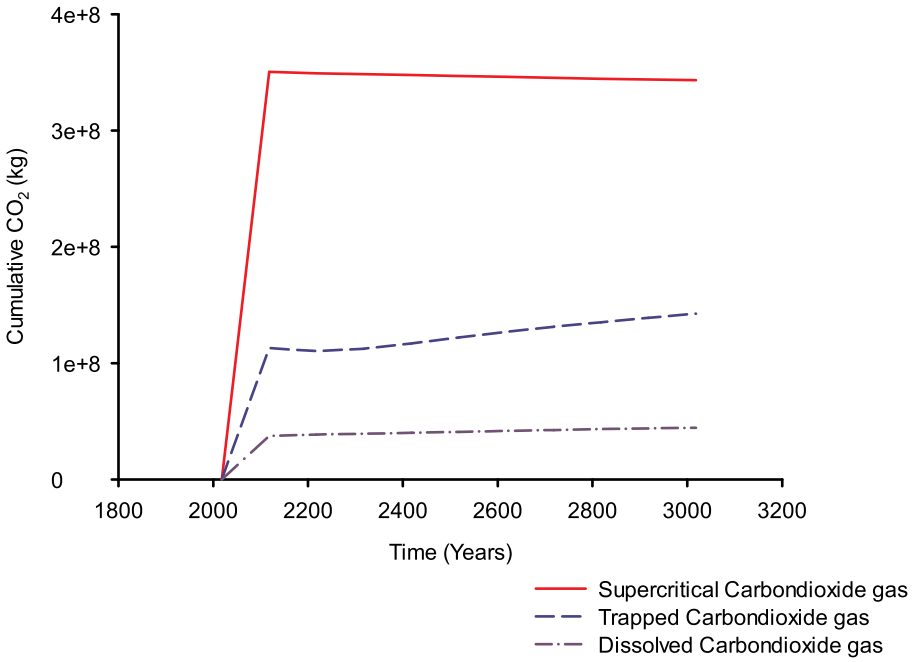

Fig. 9. Characteristic curves of different forms of cumulative CO_2 stored in 1000 years.

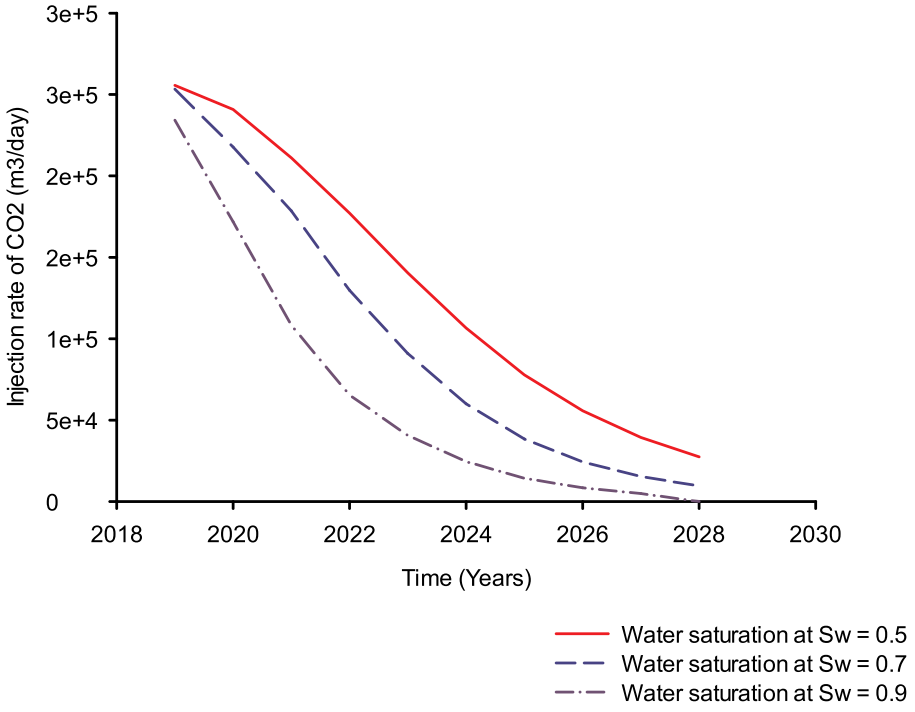

Fig. 10. CO_2 injection rates to shut-in period.

- Different formation water saturation has varying corresponding phase CO_2 storage capacity. The more the water saturation the lower the amount of CO2 to be accommodated in the reservoir. This is most likely due to the reason that saturated water limits the number of formation pores to be accessed by CO_2 in the sequestration process.
- Simulation results revealed that different CO_2 storage period has different CO_2 phase storage capacity. For example, for the simulation period of 100 years post shut-in, 73.7% of injected CO_2 was stored in form of supercritical, 20.5% as residue/trapped CO_2 and 5.8% were stored as dissolved CO_2 in the formation brine. While for a simulation period of 1000 years post shut-in, 64.8% of CO_2 was stored in supercritical form, 26.9% in trapped/residue form and 8.3% of CO_2 was stored in dissolved form.
- As far as formation water saturation is concern, it was observed that a total of 6.3×10^8 kg of CO_2 was stored at 0.5 water saturation, while 5.02×10^8 and 4.08×10^8 kg of CO_2 was stored at 0.7 and 0.9 water saturation respectively. This observation indicated a decreasing trend of total CO_2 stored compared to the amount stored at 0.5 water

Table 6
The effect of K_v/K_h to CO_2 storage, 100 years post shut-in.

K_v/K_h ratio	Supercritical CO_2 ($x10^8$) (kg)	Trapped CO_2 ($x10^8$) (kg)	Dissolved CO_2 ($x10^7$) (kg)
0.1	4.63	1.28	3.67
0.2	4.63	1.31	3.72
0.3	4.63	1.35	3.74
0.4	4.63	1.39	3.76
0.5	4.63	1.43	3.77
0.6	4.63	1.47	3.78
0.7	4.63	1.51	3.79
0.8	4.63	1.55	3.80
0.9	4.63	1.59	3.81
1.0	4.63	1.63	3.82

saturation. Therefore, water saturation has a direct effect on the storage capacity of the reservoir. Higher formation water saturation value limits reservoir pores accessibility, and hence lowers reservoir storage.

- There was an increase in CO_2 phase change storage as K_v/K_h increased. The increase of K_v/K_h ratio implied vertical reservoir permeability enhancement, and in turn, caused the migration of CO_2 in a vertical direction, and the more CO_2 migrates to the seal rock, favors interaction with the formation brine hence facilitate dissolution of CO_2.
- At higher ratios of K_v/K_h, the impact of trapped/residue CO_2 is higher compared to all other K_v/K_h ratios performed in the study. This effect led to an impact on the overall total stored amount of CO_2 in the reservoir. Simulation results revealed a total increase of 1.25 times of the cumulative amount of trapped CO_2 stored at the K_v/K_h ratio of 20 as compared to the K_v/K_h ratio of 0.5. This result reflects a 28.6% increase in the total cumulative CO_2 stored in the reservoir.
- Simulation results revealed that an increase in reservoir water salinity led to a decreased amount of dissolved CO_2 in the brine.

This study reveals that Shen 84 in Jinganbao Liaohe basin has adequate capability to store anthropogenic CO_2 at varying stages of its life as long as proper monitoring of formation pressure build-up and CO_2 plume migration control is guaranteed. Moreover, different storage period at altered water saturation has different CO_2 phase amount stored in the reservoir. The estimated safe values of this study may function as benchmark information for various similar projects in Liaohe basin or elsewhere in the world. However, detailed feasibility work needs to be conducted to increase confidence for the new CCS project start-up and implementation. This is crucial to avoid CO_2 leakage through old closed wells, fractures, and problems related to induced seismicity.

Author contributions

R.M conceived and planned the research study and set the first draft

Table 7
Effect of K_v/K_h ratio on CO_2 storage 100 years post shut-in at 0.5 water saturation.

Kv/Kh	Supercritical CO_2 ($x10^8$) (kg)	Trapped CO_2 ($x10^8$) (kg)	Dissolved CO_2 ($x10^7$) (kg)	Total Stored CO_2 ($x10^8$) (kg)
0.001	4.59	1.22	3.52	6.16
0.01	4.63	1.27	3.56	6.25
0.1	4.63	1.28	3.67	6.28
0.5	4.63	1.43	3.77	6.44
1	4.63	1.63	3.82	6.65
1.8	4.62	2.19	3.99	7.20
3	4.62	2.51	4.02	7.53
5	4.61	2.79	4.03	7.81
10	4.63	3.03	3.98	8.06
20	4.66	3.25	3.78	8.28
50	4.69	3.28	3.66	8.33
100	4.74	3.40	3.72	8.51
300	4.69	3.46	3.78	8.53
1000	4.69	3.43	3.82	8.50

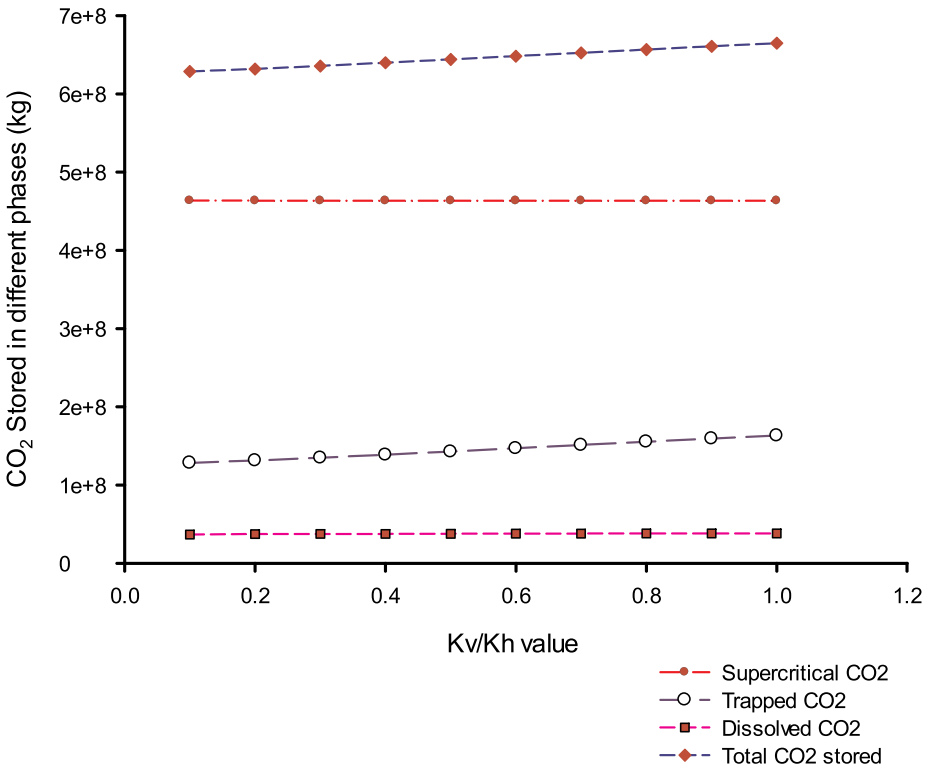

Fig. 11. Variation of CO_2 forms storage capacity based on the K_v/K_h ratio ranging from 0.1 to 1 for 100 years post shut-in.

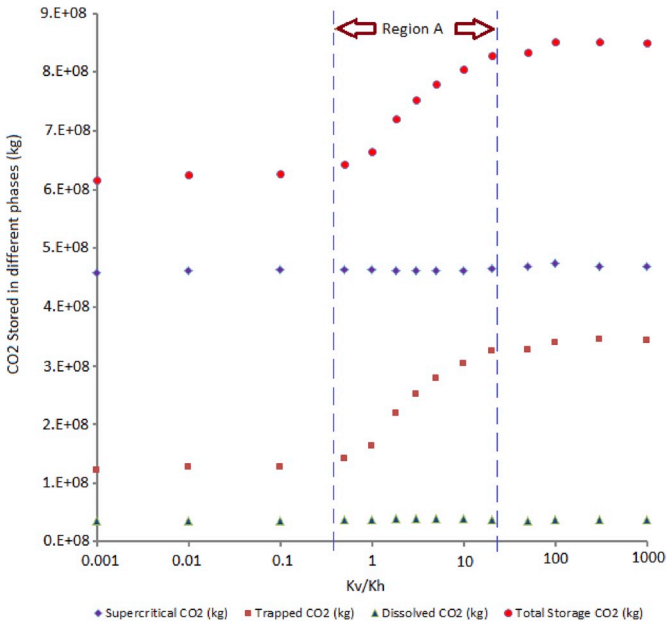

Fig. 12. Storage capacity variation caused by the change in K_v/K_h ratio tested for a water saturation range of 0.001–1000 for 100 years post shut-in.

Table 8
Parameter and values used for sensitivity analysis and their results for 100-year model simulation.

CO_2 stored in different phases with their corresponding sensitivity from the base case					
Sensitivity (Parameter)	Value	Supercritical CO_2 (%)	Trapped CO_2 (%)	Dissolved CO_2 (%)	
BHP (Mpa)	14.5	15.7	9.5	43.3	
	19.5	0.0	0.0	0.0	Base case
	24.5	48.6	48.9	21.8	
Salinity (g/L)	5	−5.3	−5.0	20.4	
	10	0	0	0	Base case
	15	12.5	11.2	−20	

of the research. G.B. supervised the research and evaluated data and results. R.M prepared the data and implemented the modeling and simulation. G.B analyzed the results and edited and revised the draft. G. B. contributed to the experiment design and data analysis.

Funding

This work was supported by the China Scholarship Council (CSC).

Declaration of competing interest

All authors declare that they do not have any conflict of interest in this study. Also, this article does not contain any studies with human participants or animals.

Acknowledgment

The authors would like to thank the China Scholarship Council (CSC) for financial support. They are also very grateful and appreciative of the technical guidance provided by all individuals during the entire study period.

Appendix A. Supplementary data

Supplementary data to this article can be found online at https://doi.org/10.1016/j.jngse.2020.103196.

References

Agada, S., Jackson, S., Kolster, C., Mac Dowell, N., Williams, G., Vosper, H., Williams, J., Krevor, S., 2017. The impact of energy systems demands on pressure limited CO 2 storage in the Bunter Sandstone of the UK Southern North Sea. Int. J. Greenh. Gas Control 65, 128–136.
Akaku, K., 2008. Numerical simulation of CO2 storage in aquifers without trapping structures. In: International Petroleum Technology Conference. International Petroleum Technology Conference.
Aminu, M.D., Nabavi, S.A., Rochelle, C.A., Manovic, V., 2017. A review of developments in carbon dioxide storage. Appl. Energy 208, 1389–1419.
Ampomah, W., Balch, R., Cather, M., Rose-Coss, D., Dai, Z., Heath, J., Dewers, T., Mozley, P., 2016. Evaluation of CO2 storage mechanisms in CO2 enhanced oil recovery sites: application to Morrow sandstone reservoir. Energy Fuels 30, 8545–8555.
Ampomah, W., Balch, R.S., Grigg, R.B., Dai, Z., Pan, F., 2015. Compositional simulation of CO2 storage capacity in depleted oil reservoirs. In: Carbon Management Technology Conference. Carbon Management Technology Conference.
Bachu, S., 2000. Sequestration of CO2 in geological media: criteria and approach for site selection in response to climate change. Energy Convers. Manag. 41, 953–970.
Bachu, S., Adams, J., 2003. Sequestration of CO2 in geological media in response to climate change: capacity of deep saline aquifers to sequester CO2 in solution. Energy Convers. Manag. 44, 3151–3175.
Basbug, B., Gumrah, F., 2007. Simulating the effects of deep saline aquifer properties for CO2 sequestration. J. Can. Petrol. Technol. 46.
CEI, S., 2011. System for Efficient Numerical Simulation of Oil Recovery. SENSOR Manual, Coats Engineering. Inc.. April 1.
CMG-GEM, 2012. Advanced Compositional and Unconventional Reservoir Simulator. Computer Modeling Group Ltd, Calgary, Alberta.
CMG-WinProp, 2012. Phase-Behaviour and Fluid Property Program. Computer Modeling Group Ltd, Calgary, Alberta.
Corey, A.T., 1954. The interrelation between gas and oil relative permeabilities. Prod. Mon. 19, 38–41.
Dai, Z., Middleton, R., Viswanathan, H., Fessenden-Rahn, J., Bauman, J., Pawar, R., Lee, S.-Y., McPherson, B., 2013. An integrated framework for optimizing CO2 sequestration and enhanced oil recovery. Environ. Sci. Technol. Lett. 1, 49–54.
Dai, Z., Viswanathan, H., Middleton, R., Pan, F., Ampomah, W., Yang, C., Jia, W., Xiao, T., Lee, S.-Y., McPherson, B., 2016. CO2 accounting and risk analysis for CO2 sequestration at enhanced oil recovery sites. Environ. Sci. Technol. 50, 7546–7554.
EPA, 2017. Inventory of US Greenhouse Gas Emissions and Sinks: 1990–2015. Washington, DC, USA, Washington, DC.
Ghanbari, S., Al-Zaabi, Y., Pickup, G.E., Mackay, E., Gozalpour, F., Todd, A.C., 2006. Simulation of CO2 storage in saline aquifers. Chem. Eng. Res. Des. 84, 764–775.
Heinemann, N., Haszeldine, R.S., Shu, Y., Stewart, R.J., Scott, V., Wilkinson, M., 2018. CO 2 sequestration with limited sealing capability: a new injection and storage strategy in the Pearl River Mouth Basin (China). Int. J. Greenh. Gas Control 68, 230–235.
Hellevang, H., Haile, B.G., Tetteh, A., 2017. Experimental study to better understand factors affecting the CO2 mineral trapping potential of basalt. Greenhouse Gases: Sci. Technol. 7, 143–157.
IPCC, 2005. Intergovernmental Panel on Climate Change Special Report on CO2 Capture and Storage Cambridge, UK.
IPCC, 2013. Climate Change 2013: the Physical Science Basis. Intergovernmental Panel on Climate Change, Working Group I Contribution to the IPCC Fifth Assessment Report (AR5). Cambridge University Press, Cambridge, United Kingdom and New York, USA.
Jia, W., McPherson, B., Pan, F., Dai, Z., Moodie, N., Xiao, T., 2018. Impact of three-phase relative permeability and hysteresis models on forecasts of storage associated with CO2-EOR. Water Resour. Res. 54, 1109–1126.
Jiang, J., Rui, Z., Hazlett, R., Lu, J., 2019. An integrated technical-economic model for evaluating CO2 enhanced oil recovery development. Appl. Energy 247, 190–211.
Jin, H., Gao, L., Li, S., van Sambeek, E., Porter, R., Mikunda, T., 2012. Supporting Early Carbon Capture Utilisation and Storage Development in Non-power Industrial Sectors. Shaanxi Province. China 12.
Kasap, E., 2001. Estimating kv/kh ratio for conductive and nonconductive shales and mudstones. In: SPE Western Regional Meeting. Society of Petroleum Engineers.
Kestin, J., Khalifa, E., Correia, J., 1981. Tables of the dynamic and kinematic viscosity of aqueous NaCl solutions in the temperature range 20-150°C and pressure range 0.1−35 MPa. J. Phys. Chem. Ref. Data 10 (1), 71–87.
Lai, Y.-T., Shen, C.-H., Tseng, C.-C., Fan, C.-H., Hsieh, B.-Z., 2015. Estimation of carbon dioxide storage capacity for depleted gas reservoirs. Energy Procedia 76, 470–476.
Leung, D.Y., Caramanna, G., Maroto-Valer, M.M., 2014. An overview of current status of carbon dioxide capture and storage technologies. Renew. Sustain. Energy Rev. 39, 426–443.
Li, Y.K., Nghiem June, L., 1986. Phase equilibria of oil, gas and water/brine mixtures from a cubic equation of state and Henry's law. Can. J. Chem. Eng. 64, 486–496.
Liu, H., Hou, Z., Were, P., Gou, Y., Sun, X., 2014. Simulation of CO 2 plume movement in multilayered saline formations through multilayer injection technology in the Ordos Basin, China. Environ. Earth Sci. 71, 4447–4462.

Liu, X., Gong, B., Huo, D., 2010. Numerical simulation on CO2 sequestration in saline formations with natural or hydraulic fractures using a discrete modeling approach. In: Canadian Unconventional Resources and International Petroleum Conference. Society of Petroleum Engineers.
Maneeintr, K., Ruanman, N., Juntarasakul, O., 2017. Assessment of CO 2 geological storage potential in a depleted oil field in the North of Thailand. Energy Procedia 141, 175–179.
Nghiem, L., Peter, S., Jim, G., Hiroshi, O., 2004. Modeling CO2 Storage in Aquifers with a Fully-Coupled Geochemical EOS Compositional Simulator. Society of Petroleum Engineers.
Nghiem, L., Shrivastava, V., Tran, D., Kohse, B., Hassam, M., Yang, C., 2009. Simulation of CO2 storage in saline aquifers. In: SPE/EAGE Reservoir Characterization & Simulation Conference.
Omambia, A.N., Li, Y., 2010. Numeric modeling of carbon dioxide sequestration in deep saline aquifers in Wangchang Oilfield-Jianghan Basin, China. J. Am. Sci. 6, 178–187.
Orodu, O.D., Tang, Z., Fei, Q., 2009. Application of prediction models to performance of high paraffinic content oilfields: case study Shen95 Block of Jinganbao Oilfield. J. Petrol. Sci. Eng. 68, 223–234.
Peng, D.-Y., Robinson, D.B., 1976a. A new two-constant equation of state. Ind. Eng. Chem. Fundam. 15, 59–64.
Peng, Y., Robinson, B., 1976b. A new two-constant equation of state. Ind. Eng. Chem. Fund. 15 (1), 59–64.
Peng, Y., Zhonghua, T., Muhammad, A.M., Ehsan, M., 2014. Study on the temperature distribution of high pour point oil by integrated method based on well log, geological data and experiment. Res. J. Appl. Sci. Eng. Technol. 7, 4945–4965.
Raza, A., Gholami, R., Rezaee, R., Bing, C.H., Nagarajan, R., Hamid, M.A., 2018. CO2 storage in depleted gas reservoirs: a study on the effect of residual gas saturation. Petroleum 4, 95–107.
Raza, A., Gholami, R., Sarmadivaleh, M., Tarom, N., Rezaee, R., Bing, C.H., Nagarajan, R., Hamid, M.A., Elochukwu, H., 2016a. Integrity analysis of CO2 storage sites concerning geochemical-geomechanical interactions in saline aquifers. J. Nat. Gas Sci. Eng. 36, 224–240.
Raza, A., Rezaee, R., Bing, C.H., Gholami, R., Hamid, M.A., Nagarajan, R., 2016b. Carbon dioxide storage in subsurface geologic medium: a review on capillary trapping mechanism. Egypt. J. Pet. 25, 367–373.
Rotty, R.M., 1983. Distribution of and changes in industrial carbon dioxide production. J. Geophys. Res.: Oceans 88, 1301–1308.
Rowe, M., Chou, S., 1970. Pressure-volume-temperature-concentration relation of aqueous NaCl solutions. J. Phys. Chem. Ref. Data 15 (1), 61–66.
Shukla, R., Ranjith, P., Haque, A., Choi, X., 2010. A review of studies on CO2 sequestration and caprock integrity. Fuel 89, 2651–2664.
Van Genuchten, M.T., 1980. A closed-form equation for predicting the hydraulic conductivity of unsaturated soils 1. Soil Sci. Soc. Am. J. 44, 892–898.
Welkenhuysen, K., Rupert, J., Compernolle, T., Ramirez, A., Swennen, R., Piessens, K., 2017. Considering economic and geological uncertainty in the simulation of realistic investment decisions for CO2-EOR projects in the North Sea. Appl. Energy 185, 745–761.
World Bank, 2017. World Development Indicators 2017. World Bank, Washington, DC.
Xiaoguang, T., Zuan, H., 1991. Buried-hill discoveries of the damintun depression in North China (1). AAPG Bull. 75, 780–794.
Xu, T., Apps, J.A., Pruess, K., 2004. Numerical simulation of CO2 disposal by mineral trapping in deep aquifers. Appl. Geochem. 19, 917–936.
Yang, Y., Li, W., Zhou, T., Dong, Z., 2018a. Using polymer alternating gas to enhance oil recovery in heavy oil. Page 012182. In: IOP Conference Series: Earth and Environmental Science. IOP Publishing.
Yang, Y., Weirong, L., Tiyao, Z., Zhenzhen, D., 2018b. Using polymer alternating gas to enhance oil recovery in heavy oil. IOP Conf. Ser. Earth Environ. Sci. 113, 012182.
Zhang, Z., 2015. Techno-economic assessment of carbon capture and storage facilities coupled to coal-fired power plants. Energy Environ. 26, 1069–1080.
Zhang, Z., Huisingh, D., 2017. Carbon dioxide storage schemes: technology, assessment and deployment. J. Clean. Prod. 142, 1055–1064.
Zhu, G., Zhang, S., Huang, H., Liu, Q., Yang, Z., Zhang, J., Wu, T., Huang, Y., 2010. Induced H2S formation during steam injection recovery process of heavy oil from the Liaohe Basin, NE China. J. Petrol. Sci. Eng. 71, 30–36.